Journal of Computational Physics **151,** 969–989 (1999)
Article ID jcph.1999.6229, available online at http://www.idealibrary.com on IDEAL®

Application of Galerkin Finite-Element Method with Newton Iterations in Computing Steady-State Solutions of Unipolar Charge Currents in Corona Devices

James Q. Feng

Wilson Center for Research and Technology, Xerox Corporation, 800 Phillips Road, Webster, New York 14580

Received October 12, 1998; revised February 3, 1999

The phenomenon of corona discharge from thin-wire or sharp-point electrodes has found various important applications especially when effective charging devices are needed. In most parts of the corona charge transport region, the unipolar charge current is established as a consequence of the drifting of ions of single polarity along the electric field lines. With negligible diffusion effects, the equation governing charge transport appears to be of hyperbolic type and has been commonly dealt with by the method of characteristics or with upwind treatments. The Poisson's equation governing the electric potential distribution in the presence of unipolar charge, on the other hand, is of elliptic type and has been conveniently dealt with by the finite-element method or the equivalent for typical boundary-value problems. The first-principle based modeling of the corona device behavior has often involved either back-and-forth iterations of solving for one of the variables with others fixed or using time integrations even when steady states are sought. In the present work, the Galerkin finite-element method is applied uniformly to all the equations in the mathematical system and the Newton iteration method is utilized to obtain quadratically converged steady-state solutions in a few steps. Straightforward application of a typical Galerkin finite-element procedure to all the equations is shown to be quite adequate, because no mechanism for boundary layer formation is present in the unipolar charge current in corona devices. Wiggle-free numerical solutions can be obtained without invoking the upwind schemes or excessive mesh refinements.

Key Words: Galerkin finite-element method; Newton iterations; steady-state solutions; corona charging; unipolar charge currents; space charge effects.

0021-9991/99 $30.00

1. INTRODUCTION

Corona discharge is a form of electrical breakdown in gases, usually occuring in the vicinity of a highly curved electrode surface where the local electric field strength becomes sufficiently large to ionize the gas molecules [1, 2]. Because the strength of the electric field decreases with distance away from the coronating electrode such as a thin wire or sharp point, the ionization zone usually remains localized around the coronating electrode surface where both positive and negative ions are generated. In the case of positive corona, i.e., the electric field is directed outward from the coronating electrode, negative ions are drawn toward the coronating electode whereas positive ions move outside the immediate vicinity of the ionization zone and drift along the electric field lines toward the collector electrode. Outside the ionization zone is the region called the drift zone, where ions of one sign dominant [3]. It is impossible to achieve static force equilibrium for every ion in a region filled with unipolar charge; ions in the drift zone are set in motion in response to the electric field. Therewith, a unipolar charge current is established. Unipolar charge currents can become an effective means for delivering charge to electrically insulated objects. The phenomenon of corona discharge from thin-wire or sharp-point electrodes has found various important applications in industrial electrostatic precipitation [4] and electrophotographic printing [5–7]. Accurate computational modeling of the electrostatic behavior of unipolar charge currents is vital to understanding the optimization of corona charging devices.

In the presence of space charge, electric potential distribution is governed by Poisson's equation, which appears to be linear with a given charge density distribution. For unipolar charge currents, however, the charge density distribution is not known *a priori* because it depends on the electric field or potential distribution. The mathematical system describing unipolar charge currents with coupled electric potential and charge density is inherently nonlinear. Solutions by analytical means are limited to a few cases where the problem configurations are highly symmetric such that the mathematical system can be reduced to an ordinary differential equation, e.g., the concentric wire-cylinder case [8]. Various approximate computational methods were used to calculate electric field and charge density in unipolar charge currents [9–11]. The Deutsch approximation that assumes the electric field lines to preserve the same shape as that determined by Laplace's equation is still a subject of study in publications of the present day [12, 13]. With the advent of powerful computers, numerical techniques for solving complicated nonlinear partial-differential equations have been developed extensively. First-principle based computations of coupled electric field and charge density for corona devices have become increasingly popular. An earlier attempt of McDonald *et al.* [14] in numerical solutions involved a straightforward finite-difference method with uniform grid in a rectangular problem domain. Despite the fact that their numerical techniques were rather primitive with some boundary conditions being apparently redundant, McDonald *et al.* successfully obtained results that compared favorably with experimental data [14].

To enable convenient computations with nonuniform mesh in complicated geometric configurations, a finite-element method was used in solving Poisson's equation with a given charge distribution [15–23]. However, some authors [18] retained the finite-difference algorithm of McDonald *et al.* [14] for solving the charge density with a given electric field, whereas most of the others [15, 19–21] replaced it with the method of characteristics because, with negligible diffusion effects, the charge transport equation for determining charge density appears to be of hyperbolic type. Over the years in corona device modelings,

the method of characteristics has been commonly used for computing the charge density distribution through the hyperbolic charge transport equation (e.g., [15, 19–21, 24–27]). The self-consistent charge density and electric field distributions have been often obtained through a scheme of back-and-forth iterative computations of charge density and electric field with one fixed while solving for the other. In combination with the method of characteristics for computing the charge density, other means besides the finite-element method for computing the electric field through Poisson's equation can also be found in the literature such as the boundary-element method [24–26], hodograph method [27], etc. The boundary-element method was sometimes considered as conceptually similar to another approach called the "charge simulation method" [28, 29].

Although popularly used as an accurate and efficient means for computing the unipolar charge density for a given electric field, the method of characteristics was found to have shortcomings such as being awkward for including multiple particle species (as often desired in modeling electrostatic precipitation devices) and not capable of modeling the diffusion effect in charge transport [30]. Hence, alternative methods were considered. For instance, Levin and Hoburg [30] developed a computational scheme using a "donor-cell" method in computing charge density with a given field and finite-element method for Poisson's equation. The apparent purpose of using the donor-cell method is to enable convenient implementation of an "upstream" difference algorithm for solving the convection dominated charge transport equation. The technique in combination with the finite-element method and donor-cell method was further improved by Adamiak [31]. Instead of using the donor-cell method with upstream difference, Takuma *et al.* [16] approached solving the charge transport equation with an upwind finite-element method. As detailed by Brooks and Hughes [32], the application of the upwind method is desired for removing spurious node-to-node oscillations or "wiggles" in numerical solutions for convection dominated second-order differential equations. For some authors uncomfortable with the upwind methods, mesh refinements for reducing the local "Peclet" number become an alternative way to achieve wiggle-free solutions. For example, in a recent paper by Medlin *et al.* [33] in taking a pseudotransient approach to a steady-state solution with the finite-volume method applied to both Poisson's equation and the charge transport equation, centered finite volume discretization was used (instead of any upwind schemes) with very fine tessellation of the problem domain and a large enough diffusion coefficient imposed to avoid numerical oscillations.

In numerical solutions for convection-dominated problems, serious wiggles typically arise from the downstream boundary where variables change rapidly [32]. The large gradients in variables are a consequence of the strong convection effect that pushes the upstream "information" toward the boundary while the downstream (Dirichlet) boundary condition forces the variables to take local values that significantly differ from the natural upstream information. Thus, a narrow boundary layer is formed at the downstream boundary where rapid changes occur. Wiggles represent spurious numerical solutions usually due to inadequate tessellation of the boundary layer. Unlike the cases with the Dirichlet condition at the downstream boundary, however, applying a Neumann condition at the downstream boundary is not likely to invoke any boundary layers, especially when a zero local normal gradient is imposed. In the absence of the boundary layers, wiggles should not be expected in the numerical solutions regardless of whether the equation contains convection-dominated terms or not. As shown in the streamline upwind/Petrov–Galerkin formulations [32], the weighted residual form of upwinding in an element is to effectively put heavier weight on the upstream node than on the downstream one. If the gradient is not large, the difference

between the upstream and downstream nodal values should be small and the weighted residuals should be insensitive to the weighting function shapes. Thus, whether an upwind scheme or mesh refinement is needed should not be determined by the appearance of a convection-dominated equation but rather should be based on the existence of mechanisms for the boundary layer to form as often controlled by the type of boundary conditions.

For unipolar charge currents in corona devices, only at the coronating (i.e., ion emitting) electrode the charge density might be controlled with reasonable certainty. In general, such a control may come from the physical mechanism of space-charged limited currents that maintains the electric field strength around the coronating electrode at a threshold value for corona onset despite the variations in the applied voltage, as often referred to as Kaptsov's assumption [34]. If the coronating electrode is a thin wire, as commonly seen in corona devices, the threshold strength of the electric field at the wire surface for corona onset is reasonably described by Peek's semi-empirical formula [35]. The application of Kaptsov's condition with Peek's formula as a boundary condition for the charge transport equation, however, has been cumbersome and several approaches have been proposed in the literature (e.g., [22]). The mathematical difficulties arise from the fact that Kaptsov's condition specifies the normal gradient of electric potential with no explicit functional connection to the charge density and therefore it cannot be directly used for specifying the charge density at the coronating wire surface. A common approach (e.g., [30, 31, 33]) is to specify a value for charge density at the wire surface and complete a solution first (called the "inner" iteration loop in [31]). Then, examine the electric field strength at the wire surface and adjust the specified value for charge density accordingly (called the "outer" iteration loop in [31]). Such an iterative procedure can usually lead to solutions with consistent charge density and electric field strength that satisfy Kaptsov's condition.

Unlike most convection diffusion problems, the charge density at outflow (downstream) boundaries, i.e., the collector electrodes, may not be tightly controlled in reality and, therefore, is not obviously known. If diffusion is neglected completely, no outflow boundary condition for charge density is needed because the charge transport equation becomes a first-order differential equation. In the charge transport equation, only the diffusion term contains the second-order derivatives. Hence, inclusion of the diffusion term requires a boundary conditions at outflow boundaries for the charge density. Descriptions of outflow boundary conditions for charge density have typically been vague in the literature. Some authors [31] specified a Neumann condition of zero normal gradient of charge density so the charge density is allowed to vary along the outflow boundary and the mathematical specification of the problem becomes complete. Physically speaking, as long as the charge density is not tightly controlled as specified in terms of the Dirichlet conditions at the outflow boundaries, charge density boundary layers are unlikely to appear in corona devices. Therefore, wiggle-free numerical solutions may be achieved in modeling unipolar charge currents in corona devices without invoking the upwind treatments or excessive mesh refinements.

Because the problem of unipolar charge currents is nonlinear, numerical solutions can be obtained only through iterations. Various iteration procedures have been used in solving nonlinear problems. Some people achieved solutions by iteratively solving one equation for one of the unknown variables with the other variables fixed (e.g., [31]). Yet, some other people obtained steady-state solutions by solving time-dependent equations via a pseudotransient approach (e.g., [33]). The usage of Newton's method of iterations has rarely been found in modeling the unipolar charge currents in corona devices. Newton's method of iterations typically renders a quadratic convergence rate and is quite robust. It is, however,

at the expense of efforts in implementing the partial derivatives in the Jacobian matrix of sensitivities of the residuals to the unknowns. Among many authors of publications in the literature, only Ghione and Graglia [22] seemed to seriously implement the Newton iteration procedure in their code with a finite-element method for Poisson's equation and a finite-box scheme for the charge transport equation. They claimed to obtain superior performance in convergence to their solutions. Applying Newton iterations to simultaneously solve electric potential and charge density was briefly mentioned by Levin and Hoburg [30]; but they did not seem to carry it out to the full extent. With the need of an extra iteration loop for adjusting the boundary condition for charge density according to Kaptsov's assumption and associated *ad hoc* treatments, the previously implemented Newton iteration procedures may still not be as complete as desired.

In the present work, the nonlinear problem of coupled electric field and unipolar charge current is discretized by means of the standard Galerkin finite-element method [36] as applied uniformly to all the equations in the mathematical system.[1] The set of nonlinear algebraic equations for steady states is solved with Newton iterations for all the unknowns simultaneously. For the convenience of initiating the Newton iterations from a trivial state (i.e., every variable takes a zero value), the diffusion term is included in the charge transport equation even though its effect is negligibly small in terms of numerical accuracy of the final solutions. The coronating electrode is considered to be a thin wire and thereby the mathematical problem is described in a two-dimensional domain. Kaptsov's condition is naturally incorporated into the boundary condition for charge density at the wire surface by introducing an auxiliary equation and an auxiliary variable. Thus, the extra iteration loop explicitly described in [31] for adjusting the charge density at the wire surface is eliminated and complete Newton iterations can be readily implemented. The reliability of the present numerical scheme is examined by comparison of computational results with the available analytical solution for the concentric wire-cylinder case. A few exemplifying results for the system of a wire enclosed in a rectangular shield are also presented.

2. GOVERNING EQUATIONS

The two-dimensional problem of unipolar charge currents considered in this work consists of a coronating wire electrode (with circular cross section) of radius R_w and one collector electrode of much larger dimension than the wire and located about $10^2 R_w$ away from the wire, as in typical configurations of corona charging devices. The medium between the wire and collector electrode is air with the permittivity of free space ϵ_0. Corona discharge occurs when the voltage applied on the wire V_w exceeds a threshold value corresponding to the corona-onset electric field strength for local air breakdown. The ionization zone where both positive and negative ions are present usually forms a uniform sheath over the surface of coronating wire [1–3]. Following the tradition in corona current modeling, the thickness of the ionization sheath is ignored, despite the fact that the validity of such a treatment may be debatable in a physical sense. Thus, a unipolar charge current can be considered in the entire region between the coronating wire surface and collector electrodes.

[1] Although rare in the literature, applying a standard finite-element method for solving the charge transport equation was described by Abdel-Salam *et al.* [17] in an early attempt in combination with a charge simulation method.

To better focus on the problem of nonlinear coupling between the electric field and space charge, air flow effects are completely ignored (as is also quite common in corona current modeling), although the "corona wind" dragged by the unipolar charge flow is well known in reality. Therefore, the dimensionless mathematical system of governing equations for electric potential V and charge density q in the steady-state unipolar charge current are Poisson's equation

$$\nabla^2 V = -q, \tag{1}$$

and the charge transport equation

$$\nabla V \cdot \nabla q - q^2 + \frac{1}{Pe_E}\nabla^2 q = 0, \tag{2}$$

where $Pe_E \equiv \mu_E V_0/D$ is the electric Peclet number with μ_E denoting the ion mobility in an electric field and D the diffusion coefficient of ions. The variables here are made dimensionless by measuring length in units of the characteristic length $L \equiv 100R_w$, electric potential in units of a characteristic voltage $V_0 \equiv 1kv$, and charge density in units of $\epsilon_0 V_0/L^2$. The corresponding dimensional forms of (1) and (2) can be found in [22, 23].

The boundary conditions for electric potential are rather straightforward to describe. At the coronating wire surface S_w and collector electrodes S_c, Dirichlet boundary conditions can be specified based on knowledge of the applied voltages. Typically, we have

$$V = V_w \text{ on } S_w \qquad \text{and} \qquad V = 0 \text{ on } S_c. \tag{3}$$

In corona current modeling, it is usually desirable to specify a value for the charge density at the coronating wire surface in terms of the Dirichlet boundary condition, i.e.,

$$q = q_w \qquad \text{on } S_w. \tag{4}$$

The knowledge about q_w, however, has been inadequate and directly specifying a physically consistent q_w in (4) is difficult. Although some people attempted to specify q_w based on empirical relationship between current and voltage measured for particular corona device, the treatments were mostly of *ad hoc* nature and not as elegant as theoretically desired in spite of the ease in computational implementation. A physically better founded approach might be to use Kaptsov's assumption [34], as often adopted in the literature. Unfortunately, the commonly accepted Kaptsov's assumption does not provide a direct description of q_w but rather it specifies that

$$\underline{\mathbf{n}} \cdot \nabla V = E_{onset} \qquad \text{on } S_w, \tag{5}$$

where E_{onset} is the threshold strength of the electric field for corona onset or local air breakdown at wire surface, with $\underline{\mathbf{n}}$ denoting the local unit normal vector that points into the wire. Traditionally (e.g., [30, 31]), to satisfy (5) in numerical solutions, a value of q_w is initially assumed in (4) so that (4) can be used as a legitimate boundary condition for charge density in solving the charge transport equation. Then, the electric field strength at the wire surface is computed from the obtained solution and its comparison with the value of E_{onset} according to (5) determines a new value of q_w for the next iteration. After many such

"outer-loop" iteractions, a consistent value of q_w can be obtained to allow the local electric field strength to eventually satisfy (5). Actually, such outer-loop iteractions are eliminated in the Galerkin finite-element scheme as detailed in Sections 3 and 4 about computational procedure. In the case where the coronating electrode is a wire, a reasonably accurate value of E_{onset} can be obtained from the nondimensionalized Peek's formula [35]

$$E_{onset} = \frac{L}{V_0}\left(A\delta + B\sqrt{\frac{\delta}{R_w}}\right), \tag{6}$$

where $A = 32.3 \times 10^5$, $B = 8.46 \times 10^4$ [33], and the $\delta = 1$ are assumed in SI units as used throughout the present paper.[2]

With the inclusion of the diffusion term, a boundary condition for charge density at the outflow boundaries should also be specified to complete the mathematical description of the problem. Because virtually no definitive knowledge is available for the charge distribution at outflow boundaries such as the collector electrodes, it is usually safe to apply a Neumann boundary condition in the Galerkin finite-element scheme for the reason discussed in Section 3. In the present work,

$$\underline{\mathbf{n}} \cdot \nabla q = 0 \qquad \text{on } S_c \tag{7}$$

is used for simplicity, where $\underline{\mathbf{n}}$ is the local normal vector at the boundaries pointing outward from the problem domain. Thus, the mechanism for establishing a boundary layer at outflow boundaries is eliminated, i.e., a sharp gradient of charge density should not appear near outflow boundaries.

At symmetry boundaries S_{sym}, if any, the boundary condition should typically be

$$\underline{\mathbf{n}} \cdot \nabla V = \underline{\mathbf{n}} \cdot \nabla q = 0 \qquad \text{on } S_{sym}. \tag{8}$$

For the problem configurations particularly considered in the present work, Eqs. (1)–(8) should be quite sufficient to form a complete mathematical system for describing the behavior of unipolar charge currents. It is straightforward to further include the Navier–Stokes equations (augmented with a term respresenting the Coulomb force) in the mathematical system for the air flow. Such an endeavor is however not pursued here for simplicity. It should be noticed that without considering the air flow and diffusion, as in most corona current models, the ion mobility μ_E virtually disappears in the steady-state mathematical system. Therefore, the results for steady electric potential and charge density distributions with negligible diffusion effects should not show any difference when the ion mobility is varied, no matter how the numerical procedures are formulated. However, the electric current density should be ion-mobility dependent, because it is a result of the product of ion mobility, charge density, and electric field.

[2] Despite the fact that Peek's formula was obtained from measurements of AC corona in a wire-cylinder system, it has been widely used in many other system configurations especially for positive DC corona from a wire (e.g., [26, 31, 33]). The justification might come from its form that has no explicit dependence on the size and shape of the collector electrode and the computational results obtained by using it often agree reasonably well with experimental data.

3. GALERKIN FINITE-ELEMENT WEIGHTED RESIDUAL FORMULATION

The nonlinear system of partial differential equations (1)–(8) is descretized by Galerkin's method of weighted residuals with finite-element basis functions [36]. In doing so, the two-dimensional problem domain (in xy space) is divided into a set of quadrilateral elements. On each element, which is mapped onto a unit square in the $\xi\eta$ (computational) domain, the unknown electric potential and charge density are each expressed in an expansion of biquadratic basis functions [36], i.e.,

$$V = \sum_i V_i \phi_i(\xi, \eta) \qquad \text{and} \qquad q = \sum_i q_i \phi_i(\xi, \eta),$$

where V_i and q_i are nodal values of V and q at node i. Galerkin's method is applied by multiplying the governing equations (1) and (2) with the same biquadratic basis functions as used for the expansions and integrating the weighted equation over the entire domain Ω. Often, the divergence theorem can be utilized to lower the order of derivatives in Poisson's equation and the diffusion term in the charge transport equation so that the Neumann boundary conditions are naturally incorporated in the weighted residual equations as surface integrals along the boundary Γ. The Galerkin method of weighted residuals transforms the nonlinear partial differential system into a set of nonlinear algebraic equations with finite degrees of freedom, to what is called the "weak form" of a system. For example,

$$R_j^V = \int_\Omega (\phi_j q - \nabla\phi_j \cdot \nabla V)\, d\Omega + \int_\Gamma \phi_j \underline{\mathbf{n}} \cdot \nabla V \, d\Gamma = 0, \tag{9}$$

$$R_j^q = \int_\Omega \left(\phi_j \nabla V \cdot \nabla q - \phi_j q^2 - \frac{1}{Pe_E} \nabla\phi_j \cdot \nabla q \right) d\Omega + \int_\Gamma \frac{1}{Pe_E} \phi_j \underline{\mathbf{n}} \cdot \nabla q \, d\Gamma = 0. \tag{10}$$

The contribution of the surface integral along Γ in (9) and (10) becomes null at S_{sym} because of (8). At S_c, when the Neumann condition is applied for q such as described in (7), the effect of the boundary condition can be negligible for large Pe_E in the residual equations (10). Because the typical value for D/μ_E is 2.66×10^{-2} volts [37], the corresponding value of Pe_E here should be 3.76×10^4 as is indeed very large. Thus, the effect of Neumann boundary conditions for q is inconsequential in the present problem, despite some uncertainties in using (7) at S_c as a boundary condition for charge density.

The Dirichlet boundary conditions (3) and (4) can be imposed by replacing the corresponding weighted residual equations ((9) and (10), respectively) associated with the boundary nodes with the specified nodal values such as $V_k = V_w$ on S_w, $V_k = 0$ on S_c, and $q_k = q_w$ on S_w, respectively. The value of q_w in (4), however, is not known *a priori*. If q_w is treated as an unknown to be determined in the solution procedure, an additional equation is needed to complete the mathematical system. Such an additional equation can be expressed in the form of an independent constraint as given in (5) according to Kaptsov's assumption.

Strictly applying Kaptsov's condition at each node on the wire surface S_w amounts to adding an equation as given in (5) at each node on S_w for determining q_w locally. Thus, q_w is generally allowed to vary along S_w and the number of extra residual equations for determining q_w is equal to the number of nodes on S_w. In implementing the Galerkin finite-element residuals, incorporating (5) as a Neumann boundary condition at S_w in the residual equations for Poisson's equation R_j^V is much more convenient because implementing a

surface integral term

$$\int_{S_w} \phi_j E_{onset}\, d\Gamma$$

in (9) is all that is needed. The auxiliary residual equations at boundary nodes on S_w are formulated in the present work as

$$R_k^a = V_k - V_w + \delta_a a_k = 0 \qquad \text{for nodes on } S_w \tag{11}$$

and nodal values of charge density on S_w are imposed according to the Dirichlet condition (4) as $q_k = a_k$ where a_k denotes the auxiliary unknowns corresponding to (11) actually as the nodal values of q_w on S_w. Ideally, δ_a should be set to zero so that a strict Kaptsov's condition can be applied. However, using (11) with $\delta_a = 0$ as the auxiliary residual equations resulted in serious oscillations in the charge density along the wire surface and a solution could not easily converge. In the present work, introducing a feedback term $\delta_a q_w$ in (11) with a small value of δ_a was found to be quite effective to circumvent the oscillation and convergence problems. To ensure numerical accuracy, the value of δ_a should of course be set as small as possible under the condition that no serious oscillations of a_k occur along S_w. As shown in Section 5, for most cases examined here, the magnitude of $\delta_a a_k$ is indeed much smaller than that of V_w and its existence in (11) is inconsequential from a practical point of view. Difficulties of obtaining a reasonably converged solution with a strictly imposed Kaptsov's condition were also reported by Ghione and Graglia [22] who suggested several approximate approaches to avoid spurious solutions. A special relaxation method was also proposed by Medlin *et al.* [33] for iteratively obtaining a charge density and field strength that consistently satisfies Kaptsov's condition (5).

4. SOLUTION PROCEDURE WITH NEWTON ITERATIONS

Discretized with the Galerkin finite-element method, the partial differential equation system of (1)–(8) becomes a set of nonlinear algebraic equations described in Section 3 as

$$\underline{\mathbf{R}}(\underline{\mathbf{u}}) \equiv \begin{pmatrix} \underline{\mathbf{R}}^V \\ \underline{\mathbf{R}}^q \\ \underline{\mathbf{R}}^a \end{pmatrix} = \underline{\mathbf{0}}, \tag{12}$$

where $\underline{\mathbf{u}} \equiv (V_1, V_2, \ldots; q_1, q_2, \ldots; a_1, a_2, \ldots)^T$, $\underline{\mathbf{R}}^V \equiv (R_1^V, R_2^V, \ldots)^T$, $\underline{\mathbf{R}}^q \equiv (R_1^q, R_2^q, \ldots)^T$, and $\underline{\mathbf{R}}^a \equiv (R_1^a, R_2^a, \ldots)^T$ as given in (9)–(11), with superscript T here denoting the transpose.

In the present work, the method of choice for solving the nonlinear equation set (12) is Newton's method of iterations [38]. Starting from an initial guess $\underline{\mathbf{u}}_{(0)}$, successive iterates are determined by

$$\underline{\mathbf{u}}_{(m+1)} = \underline{\mathbf{u}}_{(m)} + \delta\underline{\mathbf{u}} \qquad \text{with solution of } \underline{\underline{\mathbf{J}}}(\underline{\mathbf{u}}_{(m)})\delta\underline{\mathbf{u}} = -\underline{\mathbf{R}}(\underline{\mathbf{u}}_{(m)}) \tag{13}$$

where $\underline{\underline{\mathbf{J}}}$ is the Jacobian matrix of sensitivities of the residuals $\underline{\mathbf{R}}$ to the unknowns $\underline{\mathbf{u}}$, i.e.,

$$J_{ij} \equiv \frac{\partial R_i}{\partial u_j}. \tag{14}$$

At each Newton's iteration, the Jacobian matrix $\underline{\underline{\mathbf{J}}}$ is evaluated with the values of unknowns $\underline{\mathbf{u}}_{(m)}$ determined in the previous iteration and the resulting linear algebra system (13) is solved by direct factorization of the Jacobian matrix with a modification of Hood's frontal solver [39]. The iteration is continued until both the L_2 norm of residual $\|\underline{\mathbf{R}}\|$ and relative error of the solution, defined as the largest of $\max|\delta V_i|/\max|V_i|$ and $\max|\delta q_i|/\max|q_i|$, become less than 10^{-6} or $\|\underline{\mathbf{R}}\|$ alone becomes less than 10^{-10}.

Newton's method of iterations usually renders quadratic convergence to the solution. Critial here is to make an initial estimate of the solution $\underline{\mathbf{u}}_{(0)}$ that falls within the domain of convergence of Newton's method. If the diffusion term is retained in (2) with a moderate starting value of Pe_E, e.g., $Pe_E = 100$, a simple initial guess

$$\underline{\mathbf{u}}_{(0)} = \underline{\mathbf{0}} \tag{15}$$

can be used to obtain a quadratically converged solution in typically four or five steps of iterations. If a realistic value of $Pe_E = 3.76 \times 10^4$ is used, however, the diffusion term in (2) is negligibly small and (2) becomes an equation with virtually all the terms containing quadratic nonlinearities. Then, the simple initial guess (15) cannot be used because it leads to a numerically singular Jacobian matrix at the initial iteration step and solution by Newton's method, which needs the inverse of the Jacobian matrix as shown in (13), is paralyzed. Thus, implementing the diffusion term in residual equations (10) has the advantage in simple initiation of Newton iterations. Once a solution for the Pe_E of a moderate starting value is obtained, it can be used as the initial guess for the solution with a realistically large value of Pe_E or even for the case with the diffusion term in (2) or (10) completely removed. Besides using an unrealistic diffusion coefficient to initiate Newton iterations from a simple initial guess (15), other effective initialization procedures can of course be formulated. For example, the solutions shown in the present paper can also be obtained, with even the diffusion term removed, by using an initial guess $\underline{\mathbf{u}}_{(0)}$ with nodal values of V_i given by the analytic solution of Laplace's equation for the concentric wire-cylinder system, i.e.,

$$V_{(0)} = -\frac{V_w \log(x^2 + y^2)}{2\log(R_c/R_w)}, \tag{16}$$

and nodal values q_i being left as zero, assuming that the xy-coordinate origin is located at the axis of the coronating wire and $R_c/R_w = 100$.

5. EXEMPLIFYING RESULTS

The configuration of corona charging devices can vary significantly to meet various design criteria and functionality requirements. If the detailed variations are put aside, most corona charging devices may be approximated as a wire-cylinder system, where a coronating wire is enclosed in a cylindrical collector electrode. Therefore, the simplest and most studied concentric wire-cylinder system is chosen to be the first example to examine here in Subsection 5.1. Then in Subsection 5.2, the concentric wire-cylinder configuration is extended to a system with a coronating wire enclosed in a square shield, as a special configuration for corotrons used in electrophotographic processes. To represent corotrons more generally, the square shield considered in Subsection 5.2 is made rectangular in Subsection 5.3 with further analysis.

5.1. *Concentric Wire-Cylinder System*

The high degree of symmetry of the concentric wire-cylinder system enables reduction of the partial differential equation system (1)–(8) into an ordinary differential equation system that allows analytical solution. Moreover, the concentric wire-cylinder system has been considered as a prototype configuration for analysis of the electrostatic precipitator [4] and corotron in electrophotographic systems [40].

Although mathematically treating a concentric wire-cylinder system as a one-dimensional problem is quite adequate, it is computed here in a two-dimensional domain (first quadrant of the entire domain) for consistent numerical analysis and illustration. The coefficient in front of the diffusion term in (2), i.e., Pe_E^{-1}, is assumed here to be 2.66×10^{-5}, as a negligibly small number that makes no noticeable difference when compared with the computed results at $Pe_E^{-1} = 0$. The two-dimensional mesh of 400 elements used for solving the concentric wire-cylinder problem is shown in Fig. 1, where $R_c/L = 1$ and $R_w/L = 0.01$. The number of the quadrilateral elements is so chosen that the electric field strength at S_w calculated with finite-element basis function expansion has no error greater than 0.1% of the imposed value E_{onset}. Typical corotrons in electrophotographic systems use coronating wires of a diameter of about 100 μm; therefore, $R_w = 5 \times 10^{-5}$ m is assumed here. Thus, $E_{onset} = 76$, as evaluated with (6), and the corresponding voltage on the coronating wire should then be 3.4999 according to

$$V_{onset} = E_{onset} \frac{R_w}{L} \log\left(\frac{R_c}{R_w}\right). \tag{17}$$

For the case of $V_w = 5$, the L_2 norm of residual $\|\underline{\mathbf{R}}\|$ decreases from about 1 with (16) as the initial guess for V and $q_i = 0$ to the order of 10^{-1}, 10^{-2}, and 10^{-13} as Newton iterations proceed. The computed q_w is 10.494 with δ_a set to 0.001. The value of δ_a is so chosen here that node-to-node variations of q_w can only be observed at the fifth digit. For example, node-to-node variations of q_w in the present problem start to show up in the fourth digit

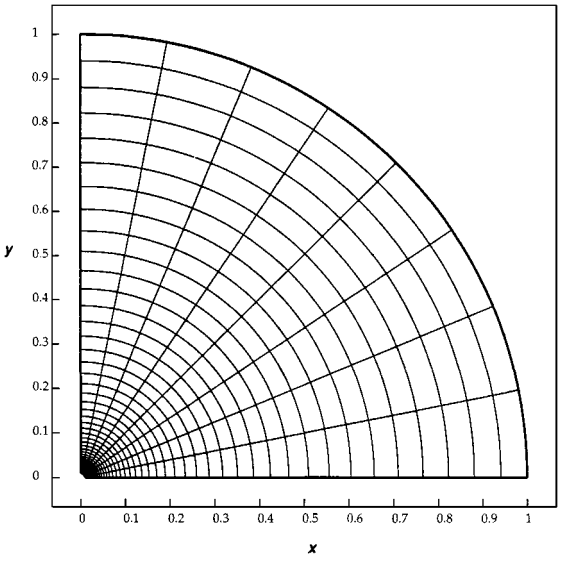

FIG. 1. Finite-element mesh for the problem of corona current in a concentric wire-cylinder system.

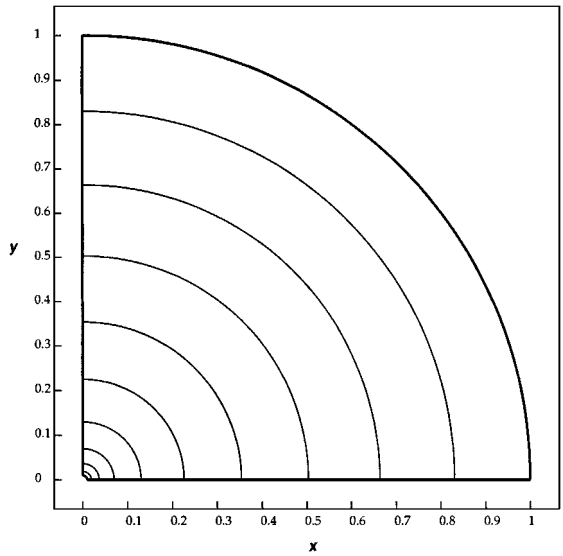

FIG. 2. Equipotentials of electric field V in a concentric wire-cylinder system with $V_w = 5$. The equipotential values are in increments of 0.5 from 0 to 4.5.

when $\delta_a = 10^{-4}$. To obtain a physically negative feedback, positive values of δ_a should be used. Because of the residual formulation (11), an increase in the nodal value of q_w results in a reduction of actual voltage imposed at S_w that effectively prevents further increase of local q_w. With $\delta_a = 0.001$ for $V_w = 5$, the actual voltage imposed on the wire surface S_w is 4.9895 instead of exact 5 (an insignificant 0.2% of change).

Figures 2 and 3 show the computed equipotential and charge density contours for $V_w = 5$, respectively. No sign of wiggles can be noticed with the charge transport equation (2) extremely convection dominated (when $Pe_E^{-1} = 2.66 \times 10^{-5}$ or even literally 0). As discussed

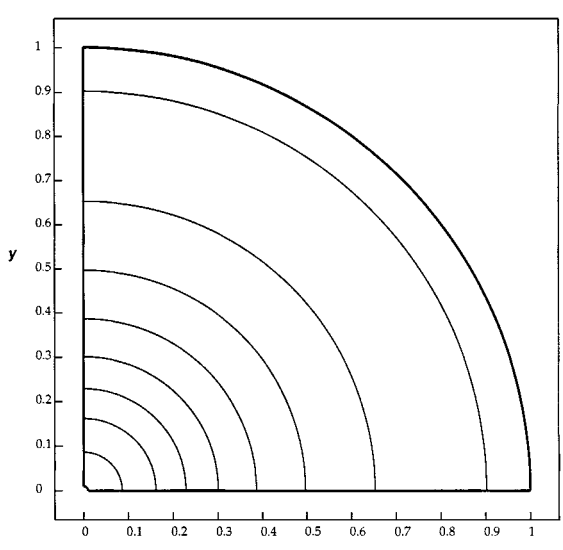

FIG. 3. Contours of space charge density q in a concentric wire-cylinder system with $V_w = 5$. The contour values are in increments of 1 from 3 to 10.

in previous sections, the applied Neuman boundary condition (7) at the outflow boundary S_c naturally becomes inconsequential as Pe_E increases to large values, by virtue of the way the Galerkin weighted residuals are formulated (cf. (10)). This is desired for mathematical consistency, because as the diffusion effect diminishes at large Pe_E the charge transport equation becomes primarily a first-order differential equation that needs only one boundary condition applied at one of the boundaries, as here with $q_k = q_w$ at S_w. If another Dirichlet boundary condition were applied at S_c, the mathematical problem approaches the singular situation or becomes the over-constraint and the picture would change completely. Figures 4a–4c show charge density contours for the same case as in Fig. 3 but with the Dirichlet boundary condition applied at S_c as $q = 2.0$, 2.5, and 2.7, respectively. For the case shown in Fig. 3, the natural value of charge density at S_c is computed as 2.7275. Not surprisingly, eye-offensing wiggles appear when the Dirichlet boundary condition is applied

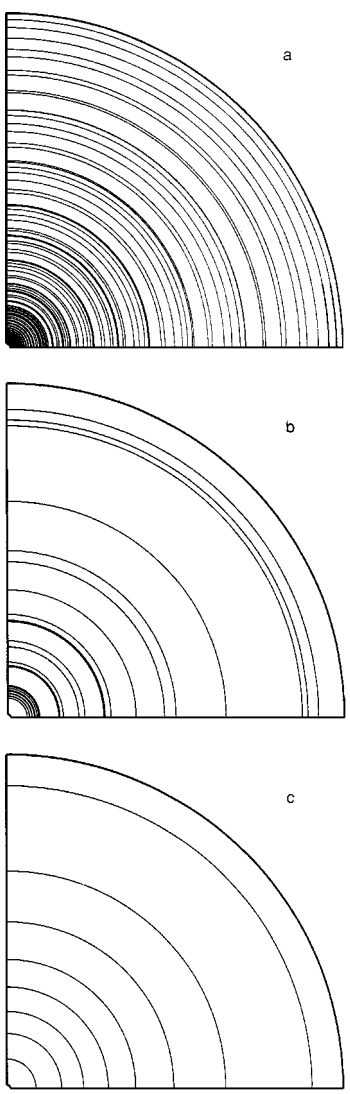

FIG. 4. Contours of space charge density q in a concentric wire-cylinder system with $V_w = 5$ and the Dirichlet boundary condition applied at S_c with (a) $q = 2.0$, (b) $q = 2.5$, and (c) $q = 2.7$. The contour values are in increments of 1 from 3 to 10.

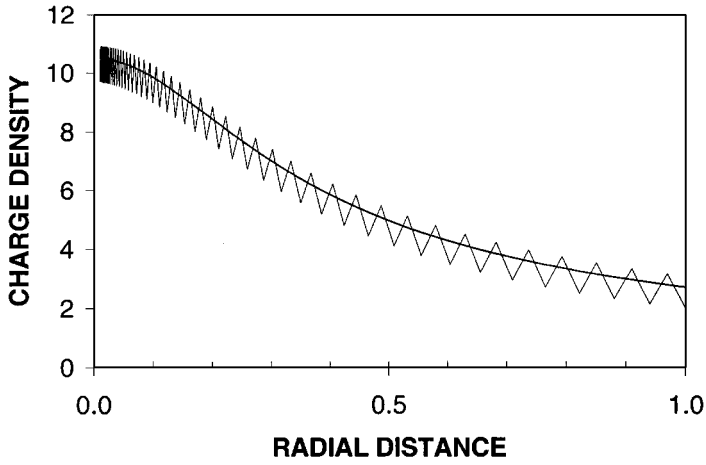

FIG. 5. Distribution of charge density q as a function of the radial distance from the wire corresponding to the solutions for Figs. 3 and 4a, to illustrate wiggles for the case when the Dirichlet boundary condition $q = 2.0$ is used.

at S_c with the boundary value of q forced away from its natural value. Well-behaved, smooth numerical solutions can only be obtrained when the boundary value of q imposed at S_c happens to be close to its natural value, as seen in Fig. 4c where $q = 2.7$. Hence, whether wiggles in the numerical solutions appear or not is not determined by the form of the convection-dominated equation but rather is based on whether the mechanisms exist for the boundary layer to form as controlled by the type of boundary conditions.

Interestingly, equipotential contours corresponding to the solution for Fig. 4a have no wiggle appearance and appear the same as Fig. 2, unlike the charge density in response to the applied Dirichlet boundary condition $q = 2$ at S_c. The reason apparently is that the electric potential relates to the charge density with twice integrations because of Poisson's equation. The integrations effectively smooth out the small-scale oscillations of wiggles.

To illustrate wiggles in q of the solution for Fig. 4a from a different perspective, Fig. 5 shows the distribution of q as a function of the radial distance from the wire, $\sqrt{x^2 + y^2}$, as $q = 2$ is applied at S_c. As a reference, the charge density distribution from the solution for Fig. 3 where $\underline{\mathbf{n}} \cdot \nabla q = 0$ is applied at S_c is also shown in Fig. 5. The center of wiggles deviates from the smooth curve because of the difference in the natural value $q = 2.7275$ and imposed value $q = 2$ at S_c. The wiggles are typical node-to-node oscillations with an amplitude of about 0.59 throughout the entire range from the wire to collector electrode.

The results shown in Figs. 2–4 indicate that the axisymmetry of the concentric wire-cylinder problem is well preserved even in the presence of serious wiggles in the two-dimensional formulation. This fact provides an independent test on the quality of the present computational scheme.

The accuracy of the present computational results can be examined by comparison with the available analytical solution for the concentric wire-cylinder problem (see, e.g., [8]). Less than 0.1% of difference is found between the computed nodal values of charge density q_i and that from the analytical formula

$$q = \frac{E_{onset}\varphi}{r\sqrt{\left[\varphi + (1-\varphi)R_w^2/(rL)^2\right]}}, \tag{18}$$

TABLE I
Comparison between Computational and Analytical Results

V_w	δ_a	q_w	φ	$f(\varphi)$	LHS of (19)
3.5	100	7.69×10^{-7}	1.01×10^{-10}	2.52×10^{-7}	1.32×10^{-4}
4	0.01	2.4283	3.1951×10^{-4}	0.62604	0.62608
5	10^{-3}	10.495	1.3809×10^{-3}	1.9599	1.9600
6	5×10^{-4}	21.828	2.8721×10^{-3}	3.2749	3.2752
7	5×10^{-4}	36.189	4.7617×10^{-3}	4.5809	4.5816

where $\varphi \equiv q_w R_w/(E_{onset}L)$ and $r \equiv \sqrt{x^2+y^2}$ are all dimensionless variables. For example, the computed nodal values of q at S_c, i.e., $r=1$, is 2.7275 and that from (18) with $q_w = 10.494$ is 2.7279.

Moreover, Table I shows the comparison of the I-V relationship between computational results and analytical formula (cf. [8])

$$\frac{V_w - V_{onset} - \delta_a q_w}{E_{onset}(R_w/L)} = f(\varphi), \tag{19}$$

where

$$f(\varphi) = (\sqrt{1-\varphi} - 1)\ln\rho + \sqrt{1+\varphi(\rho^2-1)} - 1 - \sqrt{1-\varphi}\,\ln\left[\frac{\sqrt{1+\varphi(\rho^2-1)} + \sqrt{1-\varphi}}{1+\sqrt{1-\varphi}}\right],$$

with $\rho \equiv R_c/R_w$. The value of δ_a for various V_w here is chosen based on the desire that node-to-node variations of q_w only be observed at the fifth digit. Here, the values of V_w and δ_a are imposed parameters, q_w is a computationally solved variable, and the value of φ is calculated based on the value of q_w in its definition given along with (18). The difference between the right-hand side and left-hand side (LHS) of (19) reflects slight errors in the computational results. Again, the accuracy of the computational results is quite satisfactory when compared with the analytical results. With the confidence established on the basis of the results for the concentric wire-cylinder problem, the present computational scheme is to be extended in the next subsections for corona devices that are not axisymmetric.

5.2. *Wire Enclosed in a Square Shield*

A charging device commonly used in electrophotographic printing system is called corotron, consisting of a thin wire enclosed in a shield of a rectangular cross section with one of the shield sides being the surface to be charged. The shield here serves as the charge carrier collector electrode S_c. If all the sides of the shield are of equal length, the cross section of the shield becomes square. In this subsection, the case of a wire in a square shield is computed with the radius of the wire and half side length of the square shield being the same as R_w and R_c in the last subsection for the concentric wire-cylinder problem. Thus, the value of E_{onset} remains the same. By virtue of the symmetry with the wire positioned at the center of the square, the first quadrant of the entire two-dimensional domain is computed here with a mesh of 400 elements. Because the shape of the collector electrode is not the same as a cylinder, the corona onset voltage at the coronating wire surface may differ from

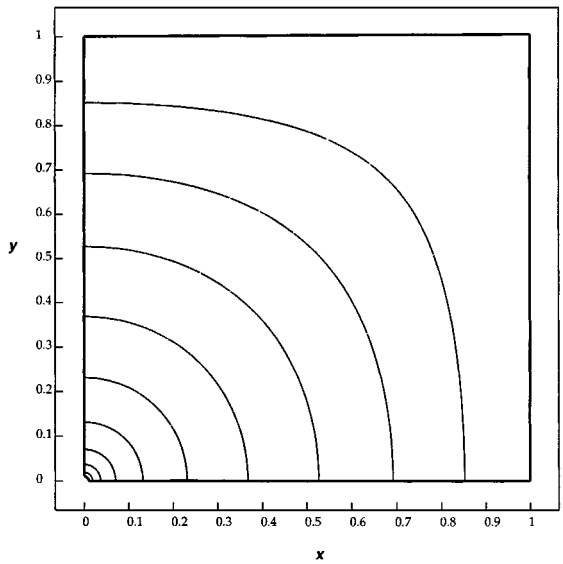

FIG. 6. Equipotentials of electric field V in the system of a wire in a square shield with $V_w = 5$. The equipotential values are in increments of 0.5 from 0.5 to 4.5.

that for the concentric wire-cylinder system. If $q_w \to 0$ is considered as an indicator of $V_w \to V_{onset}$, the value of V_{onset} can be determined by iterative computations. In the present case with $V_w = 3.558$ and $\delta_a = 100$, the computated q_w is nonuniform in the range from 5.14×10^{-6} to 5.21×10^{-6}, indicating that the value of V_{onset} for the square shield case is about 3.5575 (rather than 3.4999 for the wire-cylinder case).

Figures 6 and 7 show the computed equipotential and charge density contours for $V_w = 5$, respectively, for the case of a wire enclosed in a square shield with $\delta_a = 10^{-3}$. Although the system is not axisymmetric, the distributions of electric potential and charge density are

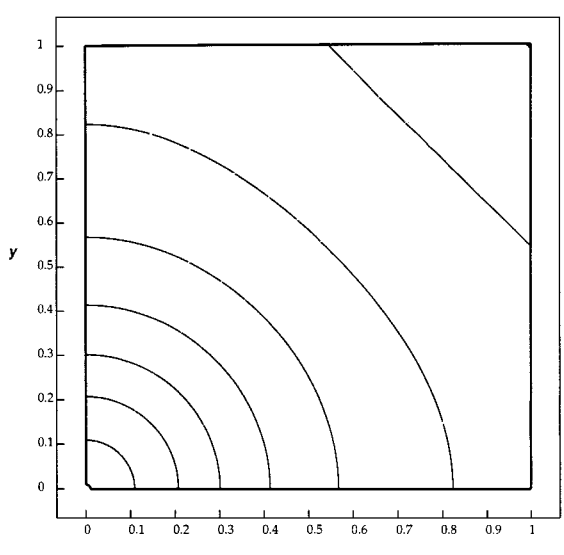

FIG. 7. Contours of space charge density q in the system of a wire in a square shield with $V_w = 5$. The contour values are in increments of 1 from 1 to 8.

quite close to the case of an axisymmetric wire-cylinder system. Nonaxisymmetric features can only be noticed in the outer region with $\sqrt{x^2+y^2} > 0.5$. The computed q_w for the square shield case, as expected to be nonuniform about the wire surface, varies in a small range from 8.5064 to 8.5139 with the minimum at 45° polar angle (i.e., at $x = y$). Even though the closest distance between the wire and shield is the same as that in the wire-cylinder case of Figs. 3 and 4, the charge density for the square shield case at $V_w = 5$ is reduced by about 20% from that for the wire-cylinder case. At $V_w = 6$ and 7 with $\delta_a = 5 \times 10^{-4}$, the computed mean values of q_w for the square shield case are around 18 and 30, respectively. For cases with R_c/L set to 2, i.e., the collector electrodes are made twice as large as those in Figs. 1–7, the computed q_w for cylindrical and square shield electrodes are 1.4783 and about 1.167, respectively at $V_w = 5$. Because the total current from a coronating wire is conserved through any equipotential surface, with the local electric field strength maintained as a constant E_{onset} according to Kaptsov's assumption and negligible diffusion effects, the value of local charge density at the wire surface q_w directly reflects the total corona current for a given constant ion mobility μ_E. Hence, the total current output from a coronating wire in a square shield is expected to the about 20% less than that in a wire-cylinder system with comparable dimensions.

5.3. *Wire Enclosed in a Rectangular Shield*

Most corotrons used in an electrophotographic system have a cross section of the rectangular shape. Therefore, a study of the case with a wire enclosed in a rectangular shield is of practical importance. For illustrative purposes, the rectangular shield considered here has reflective symmetries and only the first quadrant needs to be computed. It has one side at 1 and the other at 1.5 in terms of dimensionless distances from the wire, as shown in Fig. 8 for

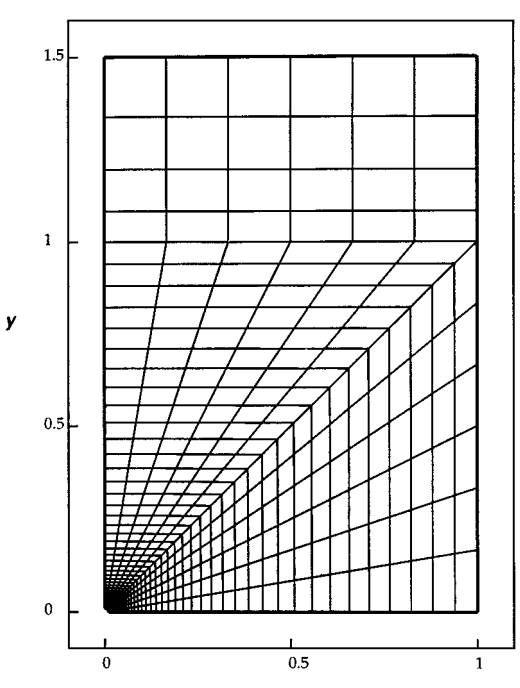

FIG. 8. Finite-element mesh for the problem of a corona current in the system with a wire enclosed in a rectangular shield.

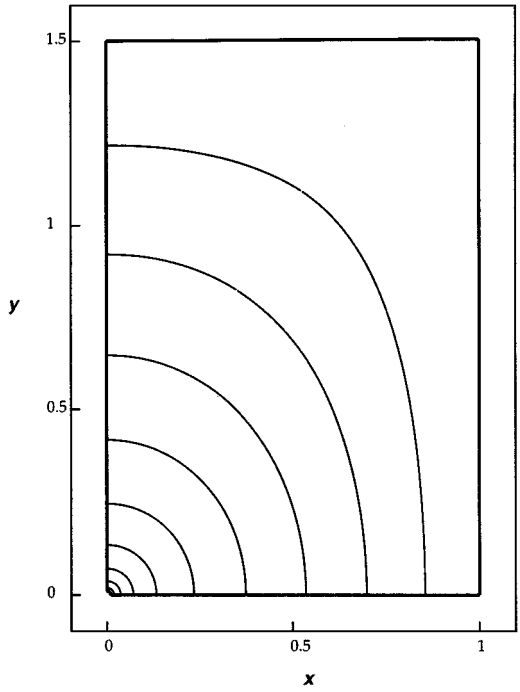

FIG. 9. Equipotentials of the electric field V in the system of a wire in a rectangular shield with $V_w = 5$. The equipotential values are in increments of 0.5 from 0.5 to 4.5.

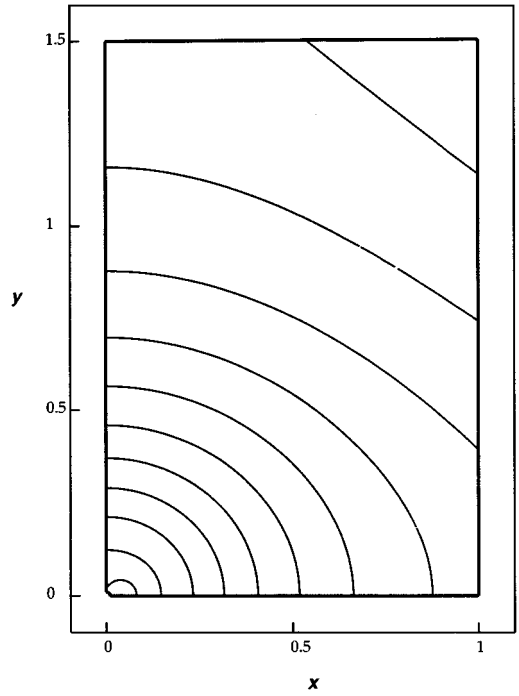

FIG. 10. Contours of space charge density q in the system of a wire in a rectangular shield with $V_w = 5$. The contour values are in increments of 0.5 from 0.5 to 5.5 and 5.8.

the tessellated domain with 624 elements. With $V_w = 3.657$ and $\delta_a = 100$, the computated q_w is in the range from 5.53×10^{-6} to 5.78×10^{-6}. Thus, the value of V_{onset} for the present rectangular shield case is about 3.6564, further increased from 3.5575 for the square shield case.

Figures 9 and 10 show the equipotential and charge density contours in the system of a wire enclosed in a rectangular shield for $V_w = 5$ with $\delta_a = 10^{-3}$, respectively, In a rectangular shield of an aspect ratio 1.5, nonaxisymmetry becomes pronounced. The nonaxisymmetric distribution of q can be seen in Fig. 10, espectially in the contour of 5.8 near the wire surface. The computed q_w for the rectangular shield case varies from 5.8089 to 5.9435 with the maximum and minimum at 0° and 90° polar angles (i.e., at x and y axes), respectively. At $V_w = 6$ and 7 with $\delta_a = 5 \times 10^{-4}$, the computed mean values of q_w for the rectangular shield case are around 13 and 22, respectively. Because one of the shield sides is further away from the wire, the total current output from the wire in the rectangular shield at the same voltage is reduced by about 30% from that for the case of the square shield.

6. CONCLUDING REMARKS

In the present work, the Galerkin finite-element method is shown to be uniformly applicable to all the equations describing the problem of unipolar space charge current in corona devices, despite the fact that the charge transport equation is convection dominated. By introducing an auxiliary equation and an auxiliary variable, Kaptsov's condition for a constant electric field strength at the coronating wire surface is naturally incorporated into the boundary condition for charge density at the wire surface. Using the Newton iteration method enables quadratical convergence of steady-state solutions such that they are obtained in a few steps. Comparison with solutions between application of Neumann and Dirichlet boundary conditions for charge density at the collector electrode demonstrates that whether wiggles in the numerical solutions appear or not is not determined by the form of the convection-dominated equation but rather by the type of boundary conditions. Because a Neumann (instead of Dirichlet) boundary condition is applied at the collector electrode in corona current problems, wiggle-free numerical solutions can be obtained without invoking the upwind schemes or excessive mesh refinements.

The accuracy of the results computed here with the Galerkin finite-element method is verified by comparison with the available analytical solution for the concentric wire-cylinder system. The results for a wire enclosed in a shield electrode of square shape show little nonaxisymmetry near the wire. If the shield electrode is made rectangular with an aspect ratio of 1.5, pronounced nonaxisymmetry is revealed in the results, especially for charge density. With the same closest distance between the coronating wire and shield electrode, the largest output corona current at a given applied voltage is obtained when a concentric cylindrical shield is used. For the same coronating wire and the same applied voltage, using a square shield would produce output corona current about 20% less than the case of a cylindrical shield. If a rectangular shield of 1.5 aspect ratio is used, the output corona current would be further reduced from the case of a square shield by about 30% for the same coronating wire and applied voltage. Even though the results computed in the present work are rather elementary for an illustration purpose, they may provide valuable theoretical guidance for the design of efficient corotrons practically used in electrophotographic printing systems.

ACKNOWLEDGMENTS

The author appreciates numerous discussions with John Facci, Ken Pietrowski, Kim Buell, Palghat Ramesh, and Meng Lean about practical and modeling issues in corotron applications.

REFERENCES

1. J. D. Cobine, *Gaseous Conductors* (Dover, New York, 1958).
2. L. B. Loeb, *Electrical Corona* (University of California Press, Berkeley, 1965).
3. R. S. Sigmond, Corona discharge, in *Electrical Breakdown of Gases*, edited by J. M. Meek and J. D. Graggs (Wiley, New York, 1978).
4. H. J. White, *Industrial Electrostatic Precipitation* (Addison–Wesley, Reading, MA, 1963).
5. J. H. Dessauer and H. E. Clark, *Xerography and Related Processes* (The Focal Press, London/New York, 1965).
6. R. Schaffert, *Electrophotography* (Focal/Hastings House, New York, 1975).
7. A. W. Baird, Positive DC coronas with arbitrary outer-conductor geometries, *IEEE Trans. Ind. Appl.* **15**(6), 676 (1979).
8. J. Q. Feng, An analysis of corona currents between two concentric cylindrical electrodes, *J. Electrostat.* **46**(1), 37 (1999).
9. N. J. Felici, Recent advances in the analysis of D.C. ionised electric fields—Part II, *Direct Currents* (Oct.) 278 (1963).
10. P. Atten, Méthode générale de résolution du probléme du champ électrique modifié par une charge d'espace unipolaire injectée, *Rev. Gén. Eléctr.* **83**, 143 (1974).
11. R. S. Sigmond, The unipolar corona space charge problem, *J. Electrostat.* **18**, 249 (1986).
12. A. Bouziane, K. Hidaka, M. C. Taplamacioglu, and R. T. Waters, Assessment of corona models based on the Deutsch approximation, *J. Phys. D* **24**, 320 (1994).
13. A. Bouziane, C. Taplamacioglu, K. Hidaka, and R. T. Waters, Non-Laplacian ion trajectories in mutually interacting corona discharges, *J. Phys. D* **30**, 1913 (1997).
14. J. R. McDonald, W. B. Smith, H. W. Spencer III, and L. E. Sparks, A mathematical model for calculating electrical conditions in wire-duct electrostatic precipitation devices, *J. Appl. Phys.* **48**, 2231 (1977).
15. W. Janischewskyj and G. Gela, Finite element solution for electric fields of coronating DC transmission lines, *IEEE Trans. Pow. Appar. Syst.* **98**(3), 1000 (1979).
16. T. Takuma, T. Ikeda, and T. Kawamoto, Calculation of ion flow fields of HVDC transmission lines by the finite element method, *IEEE Trans. Pow. Appar. Syst.* **100**(12), 4802 (1981).
17. M. Abdel-Salam, M. Farghally, and S. Abdel-Sattar, Finite element solution of monopolar corona equation, *IEEE Trans. Electr. Insul.* **18**(2), 110 (1983).
18. G. A. Kallio and D. E. Stock, Computation of electrical conditions inside wire-duct electrostatic precipitators using a combined finite-element, finite-difference technique, *J. Appl. Phys.* **59**(6), 1799 (1986).
19. J. L. Davis and J. F. Hoburg, Wire-duct precipitator filed and charge computation using finite element and characteristic methods, *J. Electrostat.* **14**, 187 (1989).
20. J. F. Hoburg and J. L. Davis, Finite element-method of characteristics computations of self-consistent charge density-electric field structures, *Comput. Electromag.* 217 (1986).
21. A. J. Butler, Z. J. Cendes, and J. F. Hoburg, Interfacing the finite-element method with the method of characteristics in self-consistent electrostatic field models, *IEEE Trans. Ind. Appl.* **25**(3), 533 (1989).
22. G. Ghione and R. D. Graglia, Two-dimensional finite-boxes analysis of monopolar corona fields including ion diffusion, *IEEE Trans. Magn.* **26**, 567 (1990).
23. M. Abdel-Salam and Z. Al-Hamouz, Finite-element analysis of monopolar ionized fields including ion diffusion, *J. Phys. D* **26**, 2202 (1993).
24. M. H. Lean and G. A. Domoto, Charge transport in viscous vortex flows, *J. Appl. Phys.* **61**(8), 3931 (1987).

25. M. H. Lean and G. A. Domoto, Charge transport in Navier–Stokes flow, *IEEE Trans. Magnet.* **24**(1), 262 (1988).
26. K. Adamiak, Simulation of corona in wire-duct electrostatic precipitator by means of the boundary element method, *IEEE Trans. Ind. Appl.* **30**(2), 381 (1994).
27. C. J. Budd and A. A. Wheeler, A new approach to the space-charge problem, *Proc. R. Soc. London A* **417**, 389 (1988).
28. M. N. Horenstein, Computation of corona space charge, electric field, and V-I characteristic using equipotential charge shell, *IEEE Trans. Ind. Appl.* **20**(6), 1607 (1984).
29. A. A. Elmoursi and G. S. P. Castle, Modelling of corona characteristics in a wire-duct precipitator using the charge simulation technique, *IEEE Trans. Ind. Appl.* **23**(1), 95 (1987).
30. P. L. Levin and J. F. Hoburg, Donor cell-finite element descriptions of wire-duct precipitator fields, charges, and efficiencies, *IEEE Trans. Ind. Appl.* **26**(4), 662 (1990).
31. K. Adamiak, Adaptive approach to finite element modelling of corona fields, *IEEE Trans. Ind. Appl.* **30**(2), 387 (1994).
32. A. N. Brooks and T. J. R. Hughes, Streamline upwind/Petrov–Galerkin formulations for convection dominated flows with particular emphasis on the incompressible Navier–Stokes equations, *Comput. Methods Appl. Mech. Eng.* **32**, 199 (1982).
33. A. J. Medlin, C. A. J. Fletcher, and R. Morrow, A pseudotransient approach to steady state solution of electric field-space charge coupled problems, *J. Electrostat.* **43**, 39 (1998).
34. N. A. Kaptsov, *Elektricheskie Yavleniya v Gazakh Vakuume* (OGIZ, Moscow, 1947).
35. F. W. Peek, Jr., *Dielectric Phenomena in High Voltage Engineering* (McGraw–Hill, New York, 1929).
36. G. Strang and G. J. Fix, *An Analysis of the Finite Element Method* (Prentice–Hall, London/New York, 1973).
37. J. R. Melcher, *Continuum Electromechanics* (MIT Press, Cambridge, MA, 1981).
38. J. M. Ortega and W. C. Rheinboldt, *Iterative Solution of Nonlinear Equations in Several Variables* (Academic Press, London/New York, 1970).
39. P. Hood, Frontal solution program for unsymmetric matrices, *Int. J. Numer. Methods Eng.* **10**, 379 (1976); Correction, *Int. J. Numer. Methods Eng.* **11**, 1055 (1977).
40. J. M. Crowley, *Fundamentals of Applied Electrostatics* (Krieger, Malabar, 1991).